



Optical harmonic generation on the exciton-polariton in ZnSe

Johannes Mund ¹, Dmitri R. Yakovlev ^{1,2}, Marina A. Semina,² and Manfred Bayer^{1,2}

¹*Experimentelle Physik 2, Technische Universität Dortmund, D-44221 Dortmund, Germany*

²*Ioffe Institute, Russian Academy of Sciences, 194021 St. Petersburg, Russia*



(Received 30 April 2020; revised 29 June 2020; accepted 7 July 2020; published 22 July 2020)

We study optical harmonic generation on the $1S$ exciton-polariton in the semiconductor ZnSe. Intense and spectrally narrow exciton resonances are found in optical second (SHG), third (THG), and fourth (FHG) harmonic generation spectra. The resonances are shifted to higher energy by 3.2 meV from the exciton energy in the linear reflectivity spectrum. Additional resonances are observed in the THG and FHG spectra and assigned to combinations of incident and backscattered photons in the crystal. Rotational anisotropy diagrams are measured and further information on the origin of the optical harmonic generation and the involved exciton states is obtained by a symmetry analysis using group theory in combination with a microscopic consideration.

DOI: [10.1103/PhysRevB.102.045203](https://doi.org/10.1103/PhysRevB.102.045203)

I. INTRODUCTION

Since the discovery of second harmonic generation (SHG) in 1961 in a quartz crystal by Franken *et al.* [1], the physics of the optical harmonic generation has developed into a mature field of both basic and applied research [2,3]. As a coherent process, SHG requires electronic states which can be excited by two-photon excitation and release one-photon emission. Additionally to fulfillment of the energy and wave-vector conservation laws, the respective optical transitions need to be allowed in electric-dipole (ED) approximation, or in higher order, like in electric-quadrupole (EQ) and/or magnetic-dipole (MD) approximation. This makes SHG a valuable and informative tool for exciton spectroscopy in semiconductors, which delivers information not available from linear optical spectroscopy approaches [4].

SHG exciton spectroscopy has been used to study various semiconductors, like GaAs [5,6], CdTe [6], ZnO [7], and Cu₂O [8]. Due to the resonant enhancement by the exciton states, the SHG signals show up as narrow lines which, at low temperatures, often are stronger than the crystallographic signals which appear also for off-resonance conditions. In these studies, magnetic and electric fields were used to reduce the symmetries of the exciton states, which gives rise to various field-induced SHG mechanisms [7,9,10]. Third harmonic generation (THG) has been also used for studying excitons, but much rarer as compared to SHG [10,11].

In bulk crystals, the strong light-matter interaction leads to the formation of exciton-polaritons with characteristic dispersions given by several polariton branches [12,13]. Nonlinear optical spectroscopy based on multiphoton excitation can be used to measure the dispersion relations of exciton-polaritons. The pioneering study on CuCl by Fröhlich *et al.* [14] revealed the upper polariton branch, measured directly by two-photon absorption (TPA). Shortly afterward, similar measurements were performed by SHG in CuCl [15–18], ZnO [17,19], and CdS [19]. Techniques using multiphoton excitation, like TPA, two-photon excitation of photoluminescence, three-photon

sum and difference frequency generation have typically more often been used for exciton-polariton studies compared to SHG (for a review, see Ref. [20]).

The semiconductor ZnSe has a large exciton binding energy of 20 meV leading to pronounced exciton-polariton properties [21,22], which makes it an attractive model system for nonlinear optical spectroscopy. Its exciton-polariton dispersion is well studied by various experimental techniques: resonant Brillouin scattering [22–24], two-photon resonant Raman scattering [25], and two-photon excitation of photoluminescence [26,27]. We showed recently that the exciton-polariton in ZnSe can be also addressed by SHG [4] and THG [11]. Note that TPA was also used in ZnSe to study the fine structure of the $2P$ exciton [28,29] and its modification in magnetic field [30–32] and under pressure [33]. Also, the second-order nonlinear susceptibility in ZnSe was investigated by SHG [34].

In this paper, we report a detailed study of optical harmonic generation (SHG, THG, and fourth harmonic generation (FHG)) on the exciton-polariton in ZnSe. We use the recently developed technique based on spectrally broad femtosecond laser pulses and signal analysis with a high-resolution spectrometer [8]. Narrow resonances are observed in the optical harmonic generation spectra that are shifted by about 3.2 meV to higher energy from the exciton resonance in the reflectivity spectrum. Rotational anisotropies of the optical harmonic generation signals are measured by rotating the linear polarizations of ingoing and outgoing photons. Their symmetries are modeled and explained in the frame of a group-theory analysis and a microscopic consideration.

The paper is organized as follows. In Sec. II, a phenomenological consideration of second, third, and fourth optical harmonic generation is given. In Sec. III, details of the experimental setup are given. The experimental results are presented in Sec. IV, and the rotational anisotropies are analyzed and discussed in Sec. V by group theory, where also the resonances in the spectra are assigned to polariton states.

II. PHENOMENOLOGICAL DESCRIPTION OF OPTICAL HARMONIC GENERATION

In semiconductors with a noncentrosymmetric crystal lattice, such as cubic ZnSe (crystallographic point group $\bar{4}3m$), the SHG process is allowed in ED approximation. The nonlinear polarization at twice the fundamental frequency, 2ω , of the exciting light for the crystallographic contribution to SHG, $\mathbf{P}^{2\omega}$, reads as

$$P_i^{2\omega} = \epsilon_0 \chi_{ijl} E_j^\omega E_l^\omega, \quad (1)$$

where i, j, l are the Cartesian indices, ϵ_0 is the vacuum permittivity, χ_{ijl} is the nonlinear optical susceptibility, $E_{j(l)}^\omega$ are the components of the electric field \mathbf{E}^ω of the laser beam at the fundamental frequency ω . Equation (1) takes into account only the resonant and nonresonant ED contributions of the electronic states in the semiconductor at the frequencies ω and 2ω . A more general approach takes into account the specifics of the material hosting exciton-polaritons. This becomes important when the SHG at frequency 2ω is in resonance with the energy of the exciton state \mathcal{E}_{exc} . To account for these contributions, the effective nonlinear polarization at double frequency 2ω , appearing under the excitation by the electric field of the electromagnetic wave $\mathbf{E}^\omega(\mathbf{r}, t) = \mathbf{E}^\omega \exp[i(\mathbf{k}^\omega \mathbf{r} - \omega t)]$, can be written in the form

$$P_{\text{eff},i}^{2\omega}(\mathcal{E}_{\text{exc}}) = \epsilon_0 \chi_{ijl}(\mathcal{E}_{\text{exc}}, \mathbf{k}_{\text{exc}}) E_j^\omega E_l^\omega, \quad (2)$$

where the nonlinear susceptibility $\chi_{ijl}(\mathcal{E}_{\text{exc}}, \mathbf{k}_{\text{exc}})$ takes into account the effects of spatial dispersion in the MD and EQ approximations. $\mathbf{k}_{\text{exc}} = 2n\mathbf{k}^\omega$ is the exciton wave vector, n is the refractive index of light at the fundamental frequency ω , and \mathbf{k}^ω is the wave vector of the incoming light. The nonlinear polarization from Eqs. (1) and (2) leads to the SHG signal with intensity $I^{2\omega} \propto |\mathbf{P}^{2\omega}|^2$.

In the case of a resonant contribution, which includes optical transitions between the ground state of the unexcited crystal $|G\rangle$ and the exciton state $|\text{Exc}\rangle$, the SHG process must be allowed both for two-photon excitation and for one-photon emission. The fulfillment of this condition depends on the symmetry of the crystal and on the geometry of the experiment. The involvement of excitons makes this picture even more complicated and interesting due to the different symmetries of the envelope wave functions of the S , P , and D exciton states, which complement the symmetry given by the point group of the crystal lattice. It is worthwhile to note here that also in case where the SHG is forbidden in ED approximation, accounting for MD and/or EQ transitions can make it allowed (see, e.g., Refs. [8,9,35]). In addition, the application of uniaxial mechanical stress, electric or magnetic fields, can lower the symmetry and can lead to optical harmonic generation on mixed exciton states that are forbidden otherwise.

A similar phenomenological approach can be applied to the THG and FHG processes. In the THG case, the effective nonlinear polarization can be written as

$$P_{\text{eff},i}^{3\omega}(\mathcal{E}_{\text{exc}}) = \epsilon_0 \chi_{ijkl}(\mathcal{E}_{\text{exc}}, \mathbf{k}_{\text{exc}}) E_j^\omega E_l^\omega E_k^\omega \quad (3)$$

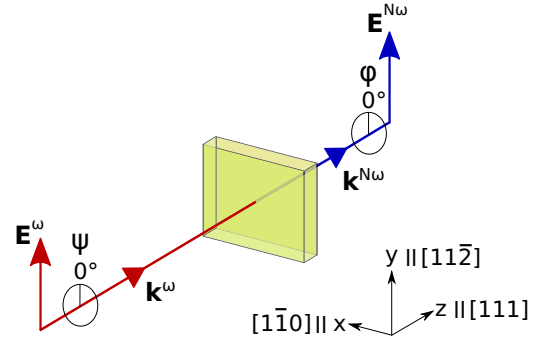


FIG. 1. Sample orientation relative to the optical axis and linear polarization angles in the optical harmonic generation experiments. Ingoing light with frequency ω and electric field component \mathbf{E}^ω has the wave vector \mathbf{k}^ω and polarization angle ψ . Generated harmonic light with frequency $N\omega$ ($N = 2, 3, 4$) and electric field component $\mathbf{E}^{N\omega}$ has the wave vector $\mathbf{k}^{N\omega}$ and can be detected at polarization angle ϕ .

and THG signal intensity is $I^{3\omega} \propto |\mathbf{P}^{3\omega}|^2$. Accordingly, for the FHG case

$$P_{\text{eff},i}^{4\omega}(\mathcal{E}_{\text{exc}}) = \epsilon_0 \chi_{ijklm}(\mathcal{E}_{\text{exc}}, \mathbf{k}_{\text{exc}}) E_j^\omega E_l^\omega E_k^\omega E_m^\omega \quad (4)$$

and FHG signal intensity is $I^{4\omega} \propto |\mathbf{P}^{4\omega}|^2$.

Generation of optical harmonics requires the fulfillment of energy and momentum conservation. The sum of energies of N ingoing photons has to be equal to the energy of the single outgoing photon, and the equivalent relations hold for the light k vectors. Here, $N = 2, 3, 4$ is the harmonic order corresponding to SHG, THG, and FHG, respectively:

$$N\hbar\omega_N = \hbar\omega^{N\omega}, \quad (5)$$

$$N\mathbf{k}_N^\omega = \mathbf{k}^{N\omega}. \quad (6)$$

In crystals where the phase-matching condition $n^{N\omega} = n^\omega$ is satisfied, the laser and harmonic beams have the same phase velocity, which leads to an amplification of the generated signal intensity. The anomalous dispersion in the range of the exciton-polariton states makes it possible to satisfy the phase-matching condition in crystals [11], while this condition is not satisfied for the nonresonant optical harmonic generation.

III. EXPERIMENT

We use a recently developed technique for exciton spectroscopy based on optical harmonic generation with 200-fs laser pulses and high spectral resolution. The technique is described in detail in Ref. [8]. In Fig. 1, the sample orientation relative to the optical axis as well as the linear polarization angles of the fundamental and harmonics light are specified.

The studied ZnSe bulk sample was grown by the Bridgman method. The sample was cut such that we can orient its crystal axes in the following way relative to the chosen coordinate axes: $[111] \parallel z$ (thickness: $2586 \mu\text{m}$), $[11\bar{2}] \parallel y$ ($4475 \mu\text{m}$), and $[\bar{1}\bar{1}0] \parallel x$ ($2458 \mu\text{m}$) (see Fig. 1). For optical measurements, the sample is kept in a bath cryostat at a temperature of $T = 5 \text{ K}$ in contact with cold helium gas.

The pump laser in our setup emits pulses of 150-fs duration at a repetition rate of 30 kHz. It pumps optical parametric amplifiers (OPA) of which one emits pulses of 3.3-ps duration and a full width at half-maximum (FWHM) of about 1 meV. The other OPA emits pulses of 200-fs duration and FWHM of about 10 meV. The OPA photon energy can be tuned in the range of relevance for the optical harmonic generation of about E_g/N , where $E_g = 2.82$ eV is the band-gap energy of ZnSe at cryogenic temperature. The energy per pulse is set to 0.1–1.0 μJ for both OPAs depending on the harmonic order to be measured.

The laser beam hits the ZnSe sample surface being parallel to the [111] crystal direction under normal incidence. It is focused into a spot with size of about 100 μm . The signals are detected by the combination of a spectrometer and a silicon charge-coupled device (CCD) camera. The 1-m Spex 1704 spectrometer has a 10×10 cm² sized grating with 1200 grooves/mm. The spectral resolution of the system in the energy range of the ZnSe band gap is 30 μeV . Further information on the detection system can be found in [9].

With a Glan-Thompson polarizer and a half-wave plate, the linear polarization of the incoming and outgoing light can be varied continuously and independently. One can thus detect the signals for any chosen polarization of \mathbf{E}^ω or $\mathbf{E}^{N\omega}$ and, therefore, measure the rotational anisotropy diagrams of the optical harmonics. In this paper, we measure these anisotropies for either parallel ($\mathbf{E}^\omega \parallel \mathbf{E}^{N\omega}$) or crossed ($\mathbf{E}^\omega \perp \mathbf{E}^{N\omega}$) linear polarizations of the laser and signal light.

In order to have information on the properties of the exciton-polaritons in the studied sample, we use linear optical spectroscopy. For measuring the reflectivity spectrum, a white-light lamp is used to illuminate the sample.

Optical harmonic generation spectra are measured by exciting the sample with laser pulses emitted by the fs OPA. With these spectrally broad fs pulses the whole spectral range around the 1S exciton can be excited by setting the central output photon energy of the OPA to \mathcal{E}_{1S}/N with corresponding N for SHG, THG, or FHG. Here, \mathcal{E}_{1S} is the energy of the exciton-polariton signal in the optical harmonic generation spectra. The spectral resolution achieved in the experiments with fs pulses depends on the detection system, as described above.

A two-photon photoluminescence excitation (2P-PLE) spectrum is recorded by detecting the photoluminescence (PL) intensity in the energy range of ± 1 meV with central energy 2.6896 eV, whereas the laser photon energy is tuned in the spectral range of the \mathcal{E}_{1S} exciton state by scanning the photon energy of the ps OPA. In this scanning regime, the spectral resolution depends on the OPA linewidth.

IV. EXPERIMENTAL RESULTS

In Fig. 2, three spectra in the energy range of the 1S exciton in ZnSe are shown. The reflectivity spectrum (blue) is plotted in Fig. 2(a). The fit (red) was made within the exciton-polariton model with taking into account the spatial dispersion in the “dead” layer approximation [12,36,37]. The evaluated “dead” layer thickness is 4.7 nm which is comparable with the exciton radius of about 3.5 nm. The fit allows to obtain the values of the exciton parameters: $E_T = 2.80268$ eV,

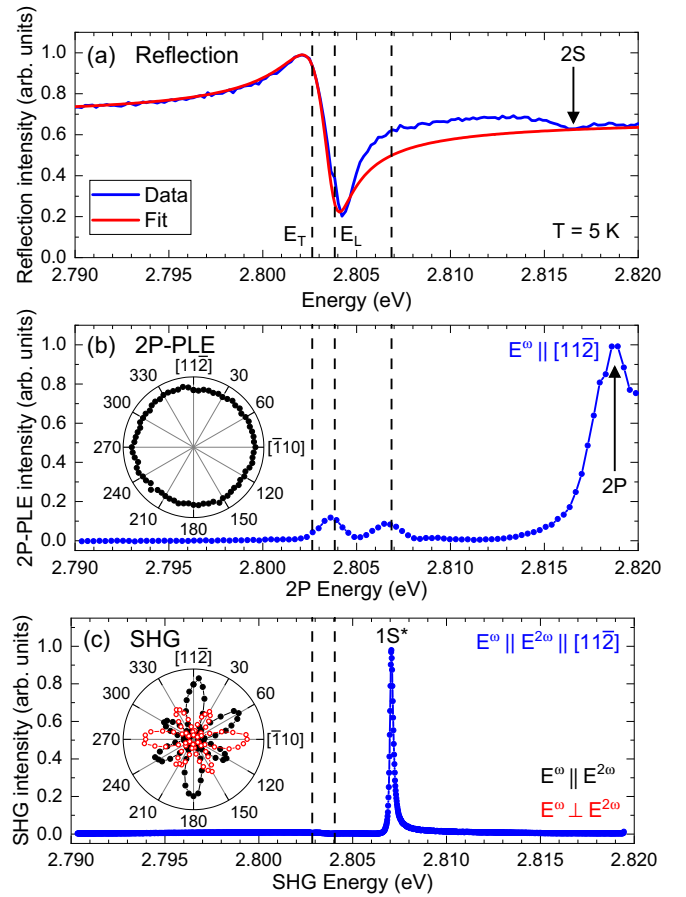


FIG. 2. Comparison of (a) white-light reflectivity spectrum, (b) 2P-PLE spectrum by ps-pulse excitation of 0.2 μJ per pulse, and (c) SHG spectrum of the 1S exciton resonance with the fundamental laser photon energy set to $\hbar\omega = 1.402$ eV (FWHM: 10 meV) and 0.1 μJ per pulse. In (a) the experimental spectrum (blue) is fitted (red) by the exciton-polariton approach described in the text. The inset in (b) shows the 2P-PLE intensity in dependence of the excitation polarization at energy $2\hbar\omega = 2.8068$ eV. The inset in (c) shows the rotational anisotropy of the SHG intensity at resonance 1S* for parallel $\mathbf{E}^\omega \parallel \mathbf{E}^{2\omega}$ (filled black dots) and crossed $\mathbf{E}^\omega \perp \mathbf{E}^{2\omega}$ (open red dots) polarization configuration.

$E_L = 2.80389$ eV, $\hbar\omega_{LT} = 1.21$ meV, and $\hbar\Gamma = 1.2$ meV. These values are in accordance with literature data [21,22,27]. We used $\epsilon = 5.5$ as the background dielectric constant and $M \approx 0.8m_0$ as exciton translational mass. Furthermore, the 2S exciton state is resolved at $\mathcal{E}_{2S} = 2.81648$ eV. The energies E_T and E_L are indicated in Figs. 2(b) and 2(c) by the dashed lines.

The 2P-PLE spectrum in Fig. 2(b) is detected at an energy of 2.68956 eV, while scanning the ps OPA. The spectrum reveals two peaks at E_L and at a higher energy of 2.8068 eV. Approaching the ZnSe band gap, another strong peak is seen at $\mathcal{E}_{2P} = 2.8188$ eV, which can be assigned to the 2P exciton state allowed for two-photon excitation [28,32]. In the inset of Fig. 2(b), the signal intensity in dependence of the polarization angle of the incoming photons \mathbf{E}^ω is presented for $2\hbar\omega = 2.8068$ eV, which shows a completely isotropic shape.

The SHG spectrum is shown in Fig. 2(c). The intense and narrow peak, labeled as 1S*, at $\mathcal{E}_{1S^*} = 2.80707$ eV dominates

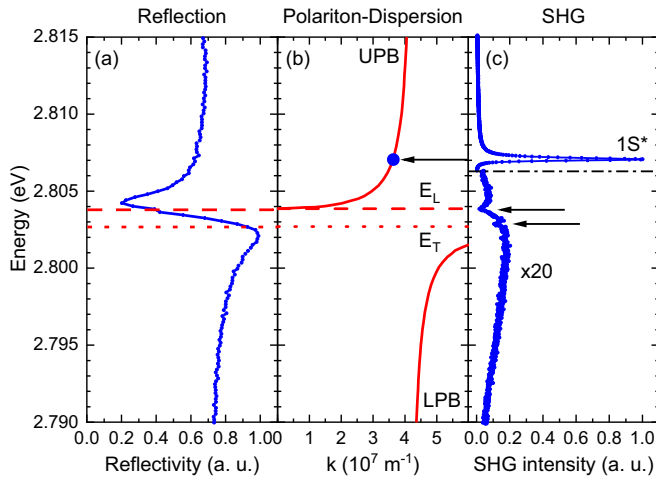


FIG. 3. Assignment of the features in the (a) reflectivity and (c) SHG spectrum to the exciton-polariton dispersion (b) [27]. The solid lines in (b) refer to the UPB and LPB. The longitudinal exciton is marked by the dashed line and the transversal exciton by the dotted line. Note that in (c) the SHG intensity in the energy range below the dashed-dotted line is magnified by a factor of 20.

the spectrum. It is also observed in the 2P-PLE spectrum in Fig. 2(b). In SHG, the FWHM of this line $\Gamma_{1S^*} = 180 \mu\text{eV}$ is not limited by the resolution of our detection system, but by inherent properties of the exciton. The rotational anisotropy of the $1S^*$ line is depicted in the inset. The full black and open red dots correspond to the parallel $\mathbf{E}^\omega \parallel \mathbf{E}^{2\omega}$ and crossed $\mathbf{E}^\omega \perp \mathbf{E}^{2\omega}$ configuration, respectively. In both configurations, a very pronounced modulation of the anisotropy can be seen, which is characteristic for the SHG signals, in contrast to the 2P-PLE that has an isotropic signal dependence on polarization of ingoing photons. The modulation originates from the crystal symmetry and is specific for the chosen crystal orientation (details will be discussed below).

We compare the reflectivity and the SHG spectrum with the exciton-polariton dispersion of the $1S$ exciton in ZnSe, taken from Ref. [27] (see Fig. 3) to assign the observed features to particular states. In Fig. 3(b), the solid lines show the exciton-polariton dispersion consisting of the upper polariton branch (UPB) and the lower polariton branch (LPB) [13]. The dashed line marks the longitudinal exciton energy, whereas the dotted line indicates the transversal exciton energy. The intense $1S^*$ resonance in the SHG spectrum is located in the UPB 3.2 meV above E_L . Furthermore, the SHG spectrum reveals two dips at $E_L = 2.80389$ eV and $E_T = 2.80268$ eV, indicating the longitudinal and transversal exciton, respectively. On the one hand, the longitudinal state can be excited by two photons, as was observed in the 2P-PLE spectrum, but does not emit light at the same energy leading to a dip in the SHG spectrum. On the other hand, the broad SHG signal below E_T is related to nonresonant SHG on the LPB.

In Fig. 4, we show SHG rotational anisotropies measured at the energy of 2.805 eV, which is between the $1S^*$ energy and E_L , and at 2.800 eV corresponding to the broad SHG signal at energies below E_T . Both anisotropies are very similar to each other and show a sixfold pattern with lobes of equal intensity.

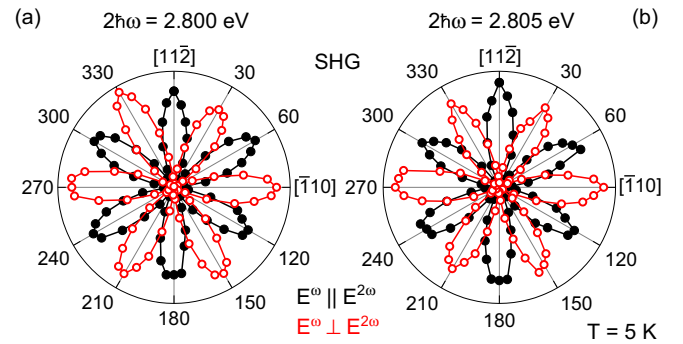


FIG. 4. SHG rotational anisotropies at the energies (a) 2.800 eV and (b) 2.805 eV. Full black and open red dots give data for parallel $\mathbf{E}^\omega \parallel \mathbf{E}^{2\omega}$ and crossed $\mathbf{E}^\omega \perp \mathbf{E}^{2\omega}$ configuration, respectively.

In Fig. 5, the THG and FHG spectra are presented along with the SHG spectrum. With increasing harmonic order, the $1S^*$ resonance is shifting to lower energy (see Table I). Furthermore, as shown in the inset, the additional small peaks r_1 and r_2 appear on the low-energy side of the $1S^*$ resonance. The r_1 resonance is not related to the longitudinal exciton state which is symmetry forbidden for one-photon emission. Further, r_1 is located at slightly higher energy, which indicates its origin on the UPB.

The rotational anisotropies of the $1S^*$ and r_1 resonances for THG and FHG are shown in Fig. 6. In THG, the anisotropy shape is almost isotropic with only a slight modulation for the parallel configuration. The intensity in the crossed configuration is much weaker and reveals a fourfold pattern with different lobe intensities. In FHG, the parallel anisotropy shows a sixfold pattern, resembling the one in SHG (compare

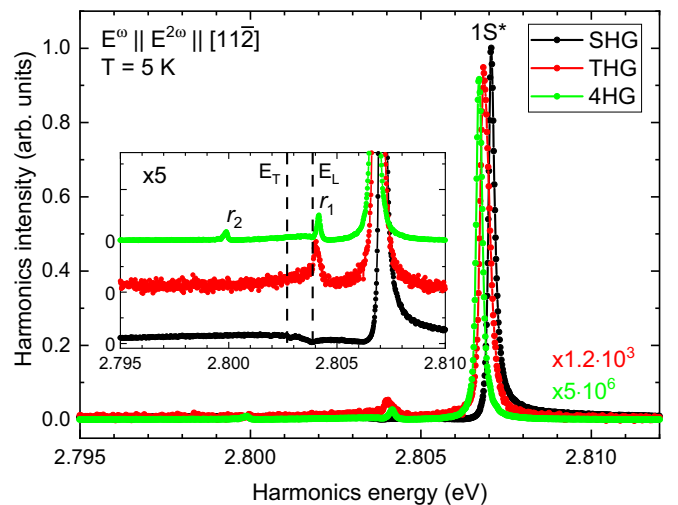


FIG. 5. SHG (black), THG (red), and FHG (green) spectra of the $1S^*$ exciton resonance. Pulse energies are $0.1 \mu\text{J}$ for SHG and THG and $1 \mu\text{J}$ for FHG. In the inset, the spectra are magnified by a factor of 5 to highlight the peaks r_1 and r_2 . Note the scaling factors of 1.2×10^3 for the THG and 5×10^6 for the FHG spectra to match the $1S^*$ resonance SHG intensity. Factors account for different excitation energies and integration times.

TABLE I. Summary of the peak energies of the $1S^*$, r_1 , and r_2 lines taken from the SHG, THG, and FHG spectra in Fig. 5 in comparison to the energies of the longitudinal and transversal exciton extracted from reflectivity. All values are given in units of eV.

Measurement	$1S^*$	r_1	r_2	E_T	E_L
Reflectivity				2.80268	2.80389
SHG	2.80707				
THG	2.80685	2.80404			
FHG	2.80671	2.80417	2.79992		

with Fig. 4). Again, the signal in crossed configuration is much weaker and does not exhibit any pronounced modulated pattern. Note that the anisotropies of the r_1 resonance in Fig. 6 have the same shape as those of the $1S^*$ line.

It is worthwhile to remind that THG energy shifts of about 0.8 and 1 meV relative to the bare exciton position were also seen in GaAs and CdTe, respectively [11]. However, ZnSe with 20-meV exciton binding energy [38] is particularly suited to observe a clear polariton shift. Similar measurements on Cu_2O with a $1S$ exciton binding energy of 150 meV [39] do not show a shift due to its different crystal symmetry and band structure. In Cu_2O , for the $1S$ exciton, one-photon optical transitions are “forbidden,” e.g., only quadrupole allowed, and excitons have lower oscillator strengths.

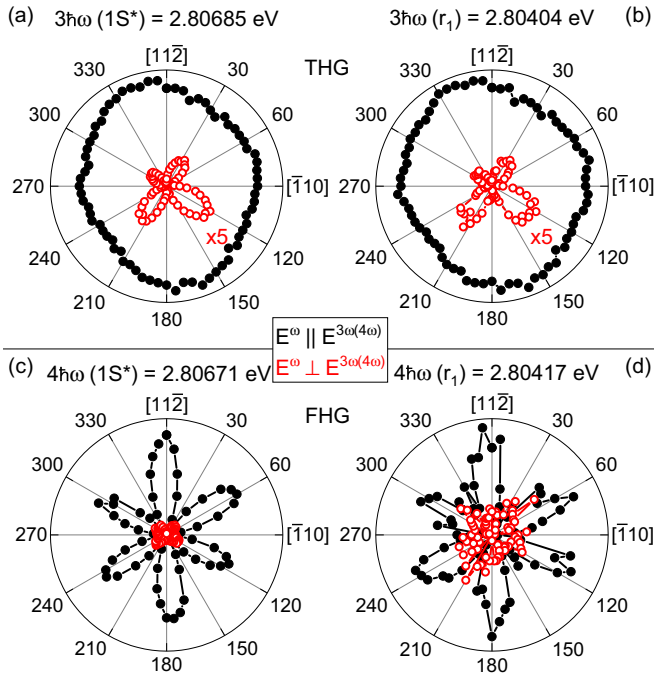


FIG. 6. Rotational anisotropies of the resonances $1S^*$ (a) and r_1 (b) in THG and in FHG (c) and (d). Full black and open red dots represent data for parallel $\mathbf{E}^\omega \parallel \mathbf{E}^{2\omega}$ and crossed $\mathbf{E}^\omega \perp \mathbf{E}^{2\omega}$ polarization configuration, respectively. Note that the crossed signal in the THG anisotropies is magnified by a factor of 5 for better visibility.

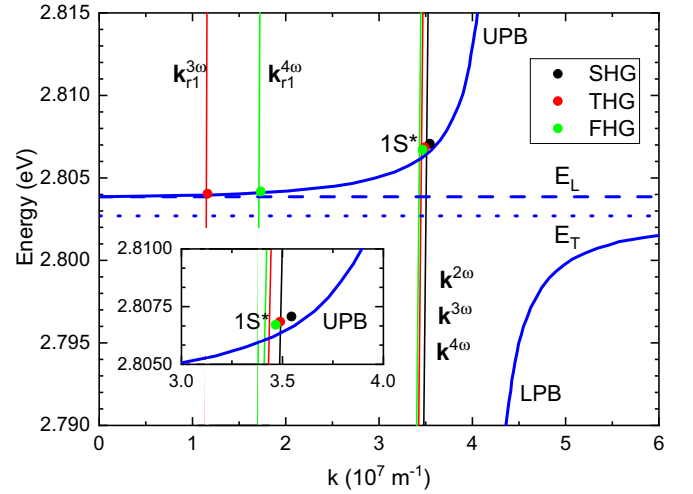


FIG. 7. Comparison of the $1S$ exciton-polariton dispersion curves consisting of the UPB and LPB (solid blue lines) and the peak positions in the harmonic measurements, shown in Fig. 5. Also, the longitudinal and transversal exciton energies (dashed and dotted blue lines) are shown. The points give the resonance energies in SHG (black), THG (red), and FHG (green). The almost vertical lines give the dispersions of the fundamental light in the corresponding harmonic measurement. The inset shows a zoom of the dispersions around the $1S^*$ resonances.

V. THEORY

In this section, we introduce first the exciton-polariton concept to explain the spectral shift of the $1S^*$ line in the optical harmonic spectra with respect to the exciton resonance in the reflectivity spectrum. Afterward, we turn to a general symmetry analysis of the optical nonlinearities in ZnSe in terms of group theory. We simulate the expected rotational anisotropies for 2P-PLE and optical harmonic generation. These are explicitly given for light directed along the $[111]$ crystal axis.

A. Exciton-polaritons

In semiconductors, strong light-matter interaction results in the formation of exciton-polaritons with a specific energy dispersion, modifying not only the linear optical properties, but also the nonlinear ones and thus the spectra of optical harmonic generation. Recently, the microscopic theory of THG on exciton-polaritons was developed for zinc-blende semiconductors and was used to describe the THG enhancement in magnetic field [11].

In Fig. 7, the dispersion of the $1S$ exciton-polariton in ZnSe with the UPB and LPB is plotted [27]. The longitudinal E_L and transversal E_T exciton energies are given by the dashed and dotted lines, respectively. A resonant signal in the optical harmonic generation spectra corresponds to the energy, where the linear light dispersion $N\mathbf{k}_N^\omega$ crosses the UPB (see the colored dots in Fig. 7). The light wave vectors \mathbf{k}_N^ω of the incoming photons can be calculated knowing the index of refraction at the respective energy $n(\hbar\omega_N)$:

$$\mathbf{k}_N^\omega = \frac{n(\hbar\omega_N)e}{c\hbar}\hbar\omega_N, \quad (7)$$

TABLE II. Summary of fundamental photon energy $\hbar\omega_N$, corresponding index of refraction $n(\hbar\omega_N)$ [40], peak energies $\hbar\omega^{N\omega}$ from Fig. 5, and $\mathbf{k}^{N\omega}$ values for SHG, THG, and FHG.

	$\hbar\omega_N$ (eV)	$n(\hbar\omega_N)$	$\hbar\omega^{N\omega}$ (eV)	$N\mathbf{k}_N^\omega$ (10^7 m^{-1})
SHG	1.40354	2.492	2.80707 (1S*)	3.545
THG	0.93562	2.453	2.80685 (1S*)	3.489
	0.93468	2.453	2.80404 (r_1)	3.485
FHG	0.70168	2.438	2.80671 (1S*)	3.467
	0.70104	2.438	2.80417 (r_1)	3.464
	0.69998	2.438	2.79992 (r_2)	3.459

where e is the elementary charge and c the speed of light. We take the $n(\hbar\omega_N)$ values for ZnSe from Table 8 in Ref. [40]. Here, the data are given for $T = 93 \text{ K}$ and are expected to be slightly larger for $T = 5 \text{ K}$.

The $n(\hbar\omega_N)$ values, used by us, are given in Table II together with the results for \mathbf{k}_N^ω of Eq. (7) for the specific photon energies of the resonances in SHG, THG, and FHG.

The harmonic resonances are given as the colored dots in Fig. 7, together with the corresponding fundamental photon dispersions. The resonances r_1 from the THG and FHG spectra are plotted at one third and at half of the calculated k values, respectively. They give access to the UPB at small k values whereas the 1S* resonances are located at larger k on the polariton dispersion [14]. The explanation is that the r_1 line arises from combinations of the ingoing photons and those which are reflected from the sample backside. Therefore, one observes the r_1 line in THG at

$$\mathbf{k}_{r_1}^{3\omega} = 2\mathbf{k}_3^\omega - \mathbf{k}_3^\omega = \mathbf{k}_3^\omega \quad (8)$$

and in FHG at

$$\mathbf{k}_{r_1}^{4\omega} = 3\mathbf{k}_4^\omega - \mathbf{k}_4^\omega = 2\mathbf{k}_4^\omega. \quad (9)$$

The 1S* resonance of each harmonic spectrum is plotted onto the dispersion of the corresponding k values: $\mathbf{k}^{2\omega}$, $\mathbf{k}^{3\omega}$, and $\mathbf{k}^{4\omega}$. For better visibility a zoom of the plot around the 1S* line positions is shown in the inset of Fig. 7.

The r_2 line is observed only in the FHG spectrum, but does not show up in SHG and THG. Its origin is not clear and requires further investigations. One can only say that it cannot be associated with Brillouin scattering from the UPB to the LPB, as for the spectral energy of 1S* in ZnSe the expected shift is about 2.5 meV (see Fig. 5 in Ref. [24]), while in our experiment the r_2 line is shifted from 1S* by 6.8 meV.

B. Symmetry analysis

ZnSe crystallizes in the zinc-blende structure of point group T_d . The structure is not centrosymmetric so that parity is not a good quantum number. SHG is allowed in ZnSe in ED approximation. The expected rotational anisotropy for nonlinear optical processes can be calculated when the symmetries of the involved electronic states are known. We take the necessary information from the tables of Koster *et al.* [41].

The symmetry of an exciton Γ_{exc} is determined by the tensor product of three irreducible representations:

$$\Gamma_{\text{exc}} = \Gamma_{\text{CB}} \otimes \Gamma_{\text{VB}} \otimes \Gamma_{\text{env}}. \quad (10)$$

Γ_{CB} and Γ_{VB} give the irreducible representations of the electron in the conduction band and of the hole in the valence band, respectively. Γ_{env} denotes the symmetry of the exciton envelope. In ZnSe, the lowest conduction band (s orbitals of Zn) has Γ_1 symmetry. If the spin is included, an electron in the conduction band is represented by Γ_6 symmetry. The uppermost valence band (p orbitals of Se) has Γ_5 symmetry which transforms to Γ_8 symmetry by spin. For the 1S exciton, the spherical envelope is of Γ_1 symmetry resulting in

$$\Gamma_{1S} = \Gamma_6 \otimes \Gamma_8 \otimes \Gamma_1 = \Gamma_3 \oplus \Gamma_4 \oplus \Gamma_5. \quad (11)$$

The symmetry Γ_3 belongs to the pure triplet paraexciton, whereas Γ_4 and Γ_5 correspond to states with singlet orthoexciton admixture.

In the point group T_d , the photon dipole operator O_D transforms as the irreducible representation Γ_5 . Thus, one photon can be absorbed by exciting a Γ_5 state, or can be emitted when a Γ_5 exciton recombines. If more than one photon is involved in the excitation process, states with other symmetries can be excited. In the case of SHG, the first photon excites virtually a Γ_5 state, whereas the second photon induces a transition from this intermediate state to a final one with Γ_1 , Γ_3 , or Γ_5 symmetry. Possible final states for single-photon and multiphoton excitation (up to four photons) are

$$1 \text{ photon} : \Gamma_5, \quad (12)$$

$$2 \text{ photons} : \Gamma_1 \oplus \Gamma_3 \oplus \Gamma_5, \quad (13)$$

$$3 \text{ photons} : \Gamma_1 \oplus \Gamma_3 \oplus 2\Gamma_4 \oplus 3\Gamma_5, \quad (14)$$

$$4 \text{ photons} : 3\Gamma_1 \oplus 2\Gamma_2 \oplus 5\Gamma_3 \oplus 6\Gamma_4 \oplus 7\Gamma_5. \quad (15)$$

For modeling the rotational anisotropies we need to consider the photons in more detail. The ingoing photons are described by their wave vector \mathbf{k}_N^ω and polarization of \mathbf{E}_N^ω . The components u_N , v_N , and w_N of the electric field \mathbf{E}_N^ω depend on the polarization angle ψ of the incoming photons (see Fig. 1). The emitted photons have the wave vector $\mathbf{k}^{N\omega}$ with components $k_x^{N\omega}$, $k_y^{N\omega}$, $k_z^{N\omega}$, and polarization along $\mathbf{E}^{N\omega}$ ($N = 2, 3, \text{ and } 4$ for SHG, THG, and FHG, respectively). The components $m^{N\omega}$, $n^{N\omega}$, and $o^{N\omega}$ depend on the outgoing polarization angle φ :

$$\mathbf{E}_N^\omega = \begin{pmatrix} u_N(\psi) \\ v_N(\psi) \\ w_N(\psi) \end{pmatrix}, \quad \mathbf{k}_N^\omega = \begin{pmatrix} k_{Nx} \\ k_{Ny} \\ k_{Nz} \end{pmatrix}. \quad (16)$$

$$\mathbf{E}^{N\omega} = \begin{pmatrix} m^{N\omega}(\varphi) \\ n^{N\omega}(\varphi) \\ o^{N\omega}(\varphi) \end{pmatrix}, \quad \mathbf{k}^{N\omega} = \begin{pmatrix} k_x^{N\omega} \\ k_y^{N\omega} \\ k_z^{N\omega} \end{pmatrix}. \quad (17)$$

C. Microscopic analysis

However, the symmetry analysis is not sufficient to predict the mechanisms that lead to the observed harmonic rotational anisotropies. A microscopic analysis is necessary to evaluate the transition probabilities to different intermediate states. This is particularly important for THG and FHG. In these cases, the final exciton state can, in principle, be excited by a manifold of excitation paths due to symmetry reasons.

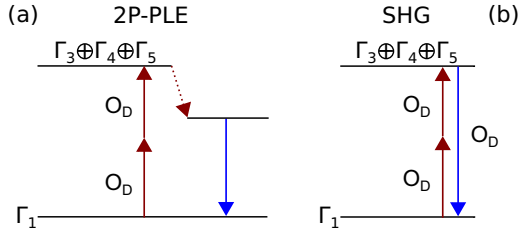


FIG. 8. (a) 2P-PLE process: excitation by two photons and emission of one photon after relaxation. (b) SHG process: coherent excitation by two photons and emission of one photon without relaxation.

We have done such a microscopic analysis, along the approach presented for THG in Ref. [11]. It allows to account for specifics of excitons and exciton-polaritons, which goes beyond the symmetry considerations based on crystal symmetries and group theory. Details of this analysis will be published elsewhere. Here, we will comment where the conclusions of microscopic analysis coincide with the group-theory considerations, and where they bring in additional information.

D. Two-photon photoluminescence excitation

Here and below we concentrate only on dominant processes. For example, we neglect quadrupole transitions if dipole transitions are allowed. Also, we neglect dipole processes which are weaker according to microscopic analysis.

The 2P-PLE process is drawn in Fig. 8(a). From Eqs. (11) and (13) we conclude that only the three components of the Γ_5 exciton can be excited by two ED transitions. States with Γ_1 and Γ_3 symmetries are not excited because the $1S$ exciton does not provide a state of Γ_1 symmetry, whereas the Γ_3 paraexciton is not accessible by ED transitions. After two-photon excitation of the Γ_5 exciton it relaxes into a lower-lying state and recombines with emission of one photon. Therefore, the emission in 2P-PLE is only dependent on the distinct polarization dependence of the excitation path.

The polarization-dependent two-photon ED transition is described by the operator O_{DD} :

$$O_{DD}(\mathbf{E}_2^\omega, \psi) = \sqrt{2} \begin{pmatrix} v_2(\psi)w_2(\psi) \\ u_2(\psi)w_2(\psi) \\ u_2(\psi)v_2(\psi) \end{pmatrix}. \quad (18)$$

For the present case of the light k vector directed along the $[111]$ crystal direction the polarization anisotropy of the 2P-PLE is measured in the $[11\bar{2}]/[1\bar{1}0]$ plane. Its explicit form is

$$O_{DD}(\mathbf{E}_2^\omega, \psi) = \frac{\sqrt{2}}{3} \begin{pmatrix} -\cos(\psi)[\cos(\psi) + \sqrt{3}\sin(\psi)] \\ \cos(\psi)[-\cos(\psi) + \sqrt{3}\sin(\psi)] \\ \frac{1}{2}[-1 + 2\cos(2\psi)] \end{pmatrix}. \quad (19)$$

The detected PL intensity is proportional to the square of O_{DD} :

$$I^{2P-PLE} \propto |O_{DD}(\psi)|^2. \quad (20)$$

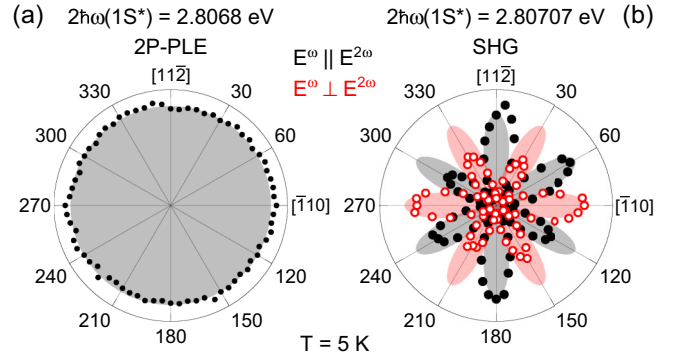


FIG. 9. (a) Measured 2P-PLE data (full black dots) at the $1S^*$ line and simulation by Eq. (20) (gray shaded area). (b) Full black and open red dots are measured SHG data at the $1S^*$ resonance for parallel $\mathbf{E}_2^\omega \parallel \mathbf{E}^{2\omega}$ and crossed $\mathbf{E}_2^\omega \perp \mathbf{E}^{2\omega}$ configuration, respectively. Gray and red shaded areas represent the simulations by Eq. (22).

Note that, despite the form of Eq. (19), I^{2P-PLE} is a constant function for all ψ and thus gives an isotropic pattern for the rotational diagram.

The measured rotational anisotropy of 2P-PLE on the $1S^*$ line, shown in the inset of Fig. 2(b), is compared with model calculations in Fig. 9(a), where the simulation by Eq. (20) is given by the gray shaded area.

E. Second harmonic generation

For SHG, the two-photon excitation process is the same as in 2P-PLE and is followed by the one-photon emission from the same state. Therefore, additional selection rules are due compared to 2P-PLE. The operator for one-photon emission along the $[111]$ direction is given by

$$O_D(\mathbf{E}^{2\omega}, \varphi) = \frac{1}{\sqrt{6}} \begin{pmatrix} \cos(\varphi) - \sqrt{3}\sin(\varphi) \\ \cos(\varphi) + \sqrt{3}\sin(\varphi) \\ 2\cos(\varphi) \end{pmatrix}. \quad (21)$$

Note that the same operator is valid for the one-photon emission in THG and FHG processes considered below. The SHG intensity is calculated by

$$I^{2\omega} \propto |O_{DD}(\psi)O_D(\varphi)|^2. \quad (22)$$

Thus, we expect a sixfold pattern for both parallel and crossed configurations, which are, however, rotated by 30° with respect to each other. In Fig. 9(b), the experimental SHG rotational anisotropies at the $1S^*$ resonance are compared with the simulations according to Eq. (22). The parallel and crossed configurations are realized by fixing $\varphi = \psi$ and $\varphi = \psi + 90^\circ$, respectively.

As can be seen in Fig. 9(b), the SHG signal, measured on the $1S^*$ line, shows general agreement, but also has some deviations from the modeling. In particular, the sixfold pattern of the simulation is reproduced, but with varying intensities of the individual lobes. On the one hand, this finding can be explained by the potential presence of residual strain in the sample. Strain can provide a splitting of the ideally threefold-degenerate Γ_5 exciton. Then, interference of the emission from the two transversal and the longitudinal exciton state

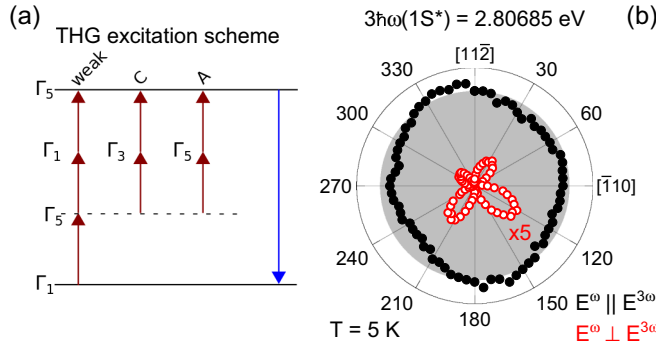


FIG. 10. (a) Excitation paths for Γ_5 excitons in THG. The dashed line is a guide to the eye for the virtually excited intermediate state. Arrows represent photon transitions of Γ_5 symmetry. (b) Full black and open red dots are measured THG data at the $1S^*$ line for parallel $\mathbf{E}_3^\omega \parallel \mathbf{E}^{3\omega}$ and crossed $\mathbf{E}_3^\omega \perp \mathbf{E}^{3\omega}$ configuration, respectively. The gray shaded area represents the simulation by Eq. (24) with the ratio $C/A = 1$.

has to be taken into account, as shown for Cu_2O [35]. The parameters of the exciton splittings under uniaxial stress in ZnSe can be found in Ref. [27]. On the other hand, also a small deviation of \mathbf{k}_V^ω from the [111] direction can induce mixing of the exciton states. Note that the 2P-PLE rotational anisotropy is not affected by interference because prior to emission, the excitation relaxes into an energetically lower state. During this process, the information about k vector and polarization of the excitation is not conserved and, therefore, the coherence is lost.

A second possible reason for the mismatch between the SHG experiment and modeling can be photon processes beyond the ED approximation. Additionally to the considered ED transitions, EQ and/or MD transitions may contribute

to SHG [8,9]. For example, the Γ_5 exciton can be excited by two photons in ED order and emit a photon in ED or EQ order, which can interfere resulting in a modified rotational anisotropy.

The microscopic analysis coincides with the group-theory approach for SHG. There is only one path due to symmetry by which the Γ_5 $1S$ exciton can be excited in ED approximation. Also, there is only one independent tensor component χ_{xyz} [13]. An in-depth microscopic analysis reveals that the first photon of the two-photon excitation path in SHG virtually excites a remote band before the second photon excites the $1S$ exciton.

F. Third harmonic generation

THG differs from SHG by the increased number of photons in the excitation process. Therefore, as shown in Eq. (14), also states of symmetry Γ_4 can be excited by three photons. Furthermore, additional excitation paths become available for states of a certain symmetry due to the increased number of intermediate states, which are virtually excited by the photons. This number of paths is given by the coefficients in Eq. (14). Let us discuss the case of $3\Gamma_5$ as an example, which is illustrated in Fig. 10(a). By two photons, states of Γ_1 , Γ_3 , and Γ_5 symmetry can be virtually excited. From each of these states an additional photon of Γ_5 symmetry can excite the final $1S$ Γ_5 state. Thus, the increased number of excitation paths can lead to signals of different polarizations, which can interfere with each other. However, a microscopic analysis of the different paths accounting only for interband transitions and excluding transitions to remote bands gives further information about the strengths of each excitation [11]. Analysis shows that the paths via states Γ_3 and Γ_5 are strongest.

The three-photon excitation operator for the light k vector directed along the crystal [111] direction is given by

$$O_{\text{DDD}}(\mathbf{E}_3^\omega, \psi, A, C) = \frac{1}{6\sqrt{6}} \begin{pmatrix} 2(A-C)\cos(3\psi) + (3A+C)[\cos(\psi) - \sqrt{3}\sin(\psi)] \\ 2(A-C)\cos(3\psi) + (3A+C)[\cos(\psi) + \sqrt{3}\sin(\psi)] \\ 4\cos(\psi)[-2A + (A-C)\cos(2\psi)] \end{pmatrix}. \quad (23)$$

The parameters A and C give the strength of the paths via Γ_5 and Γ_3 , respectively. They can be assigned to tensor components $A = \chi_{xxyy}$ and $C = \chi_{xxxx}$ as in Ref. [11].

Thus, the THG intensity is calculated according to

$$I^{3\omega}(A, C) \propto |O_{\text{DDD}}(\psi, A, C)O_{\text{D}}(\varphi)|^2. \quad (24)$$

A comparison of the THG rotational anisotropies at the $1S^*$ resonance with simulations using Eq. (24) for $C/A = 1$ is shown in Fig. 10(b). For the parallel configuration, an isotropic signal intensity is expected from Eq. (24) whereas in the crossed configuration no signal is allowed. In the measurement, a slight deviation of the parallel signal from the expected one is observed and, furthermore, weak THG intensity with a fourfold pattern is present in the crossed configuration. Deviations from the expected shape might be explained by strain in the sample which can disturb the crystal symmetry, or processes beyond the ED approximation.

In Ref. [11], the THG signal in GaAs deviated from the isotropic shape and was fitted with $C/A = 0.82$.

In Figs. 11(a) and 11(b), we show expected anisotropy shapes for the two paths, denoted by A and C , for $\mathbf{k}^\omega \parallel [111]$ and $\mathbf{k}^\omega \parallel [001]$ crystal direction. Figure 11(c) shows the interference of both paths with $A = C$. The shapes are calculated by Eq. (24) with O_{DDD} from Eqs. (24) and (A9), respectively. Particularly for the [001] direction it is interesting and instructive, that each individual path via either Γ_3 or Γ_5 state results in strongly modulated diagrams, whereas their interference for the case $A = C$ results in an isotropic pattern.

G. Fourth harmonic generation

In the case of FHG, four photons are involved in the excitation providing a variety of intermediate states and excitation paths. The possible paths for a Γ_5 exciton in FHG are depicted in Fig. 12. From the symmetry calculation, several paths can

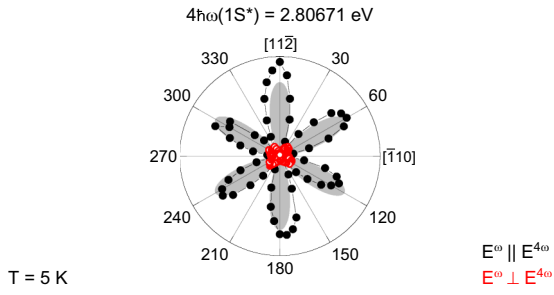


FIG. 13. Full black and open red dots give measured FHG data at the $1S^*$ resonance for parallel $E^\omega \parallel E^{4\omega}$ and crossed $E^\omega \perp E^{4\omega}$ configuration, respectively. The gray shaded area represents the simulation for parallel configuration by Eq. (26). No signal is expected in crossed configuration.

VI. CONCLUSIONS

We have extended the recently developed approach of SHG spectroscopy by excitation with spectrally broad femtosecond laser pulses and spectrally resolved detection for SHG, THG, and FHG studies of exciton-polaritons in the semiconductor ZnSe. The observed spectral shift of the optical harmonic generation signals from the exciton resonance in the reflectivity spectrum of about 3.2 meV is well described by the exciton-polariton dispersion. The experimentally measured rotational anisotropies for light propagation along the $[111]$ crystal axis are in good agreement with the group-theory modeling. We provide simulations also for other crystal orientations and show that, e.g., the SHG is symmetry forbidden for $[001]$ orientation, for which therefore application of an external magnetic field is promising to induce magnetic-field-induced SHG signals. The developed approach can be readily extended for other semiconductors and semiconductor heterostructures,

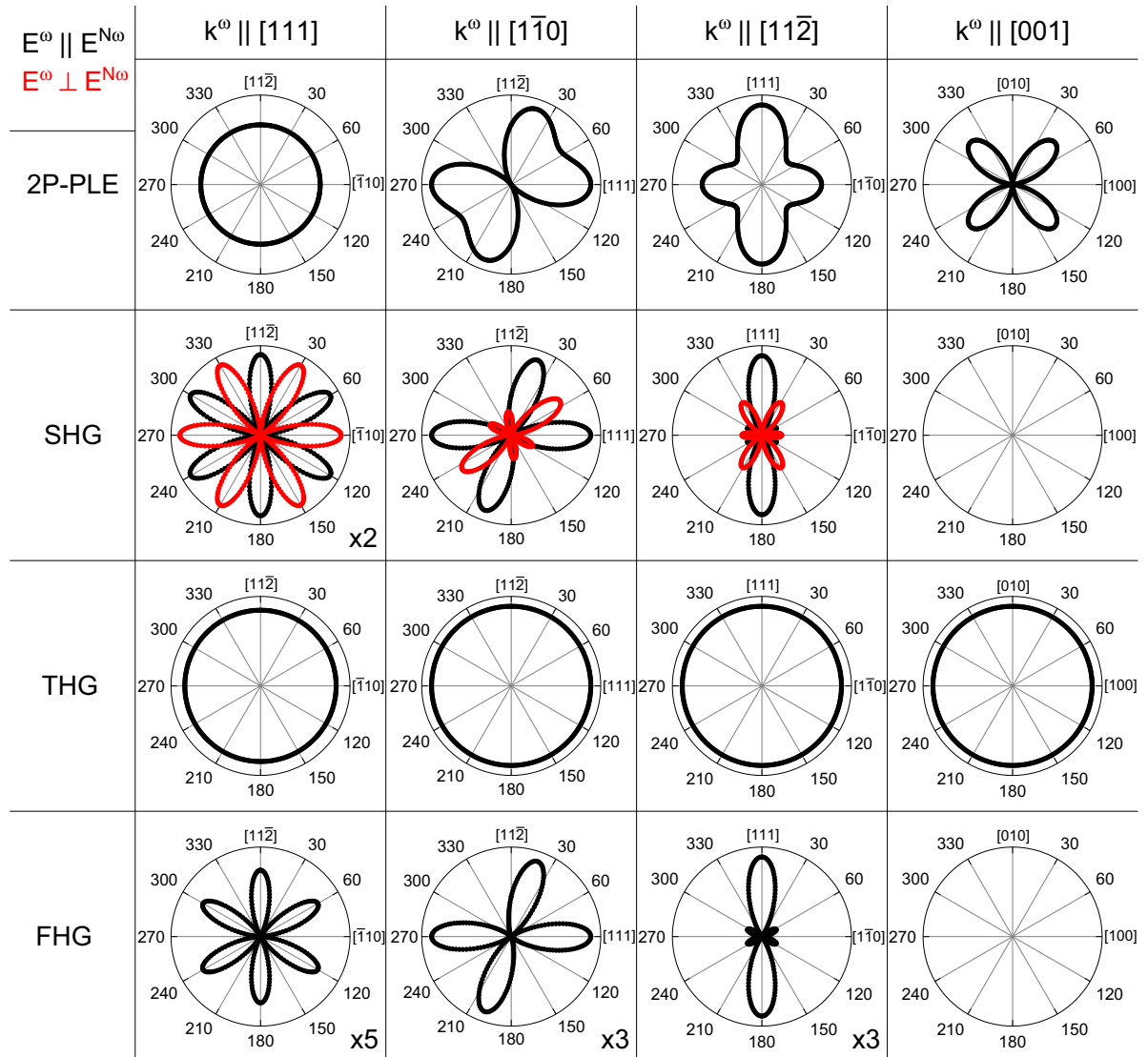


FIG. 14. Calculation of rotational anisotropies for S excitons of Γ_5 symmetry in 2P-PLE, SHG, THG, and FHG for several crystal orientations. Black and red lines give the simulations for parallel $E^\omega \parallel E^{N\omega}$ and crossed $E^\omega \perp E^{N\omega}$ configuration, respectively. THG anisotropies are calculated using $A = C$.

e.g., for exciton-polaritons in microcavities in the strong coupling regime.

ACKNOWLEDGMENTS

The authors are thankful to D. Fröhlich, M. M. Glazov, and E. L. Ivchenko for fruitful discussions. We acknowledge the financial support by the Deutsche Forschungsgemeinschaft through the International Collaborative Research Centre TRR 160 (Project C8) and the Collaborative Research Centre TRR 142 (Project B01). M.A.S. also acknowledges the partial financial support by the Russian Foundation of Basic Research, Projects No. 19-52-12063 and No. 19-52-12038.

APPENDIX: FORMULAS FOR ANISOTROPY SIMULATION

Here, we give the explicit forms of the operators O_D which give the one-photon emission and O_{ND} for excitation in the different harmonic orders. Formulas are shown for $\mathbf{k}_N^\omega \parallel [1\bar{1}0]$, $[11\bar{2}]$, and $[001]$. Note that O_{DD} is the same for 2P-PLE and SHG since in both cases excitation is done by two photons.

1. One-photon emission

One-photon emission operator for $\mathbf{k}^{N\omega} \parallel [1\bar{1}0]$:

$$O_D(\mathbf{E}^{N\omega}, \varphi) = \frac{1}{\sqrt{6}} \begin{pmatrix} \cos(\varphi) + \sqrt{2} \sin(\varphi) \\ \cos(\varphi) + \sqrt{2} \sin(\varphi) \\ -2 \cos(\varphi) + \sqrt{2} \sin(\varphi) \end{pmatrix}. \quad (\text{A1})$$

One-photon emission operator for $\mathbf{k}^{N\omega} \parallel [11\bar{2}]$:

$$O_D(\mathbf{E}^{N\omega}, \varphi) = \frac{1}{\sqrt{6}} \begin{pmatrix} \sqrt{2} \cos(\varphi) + \sqrt{3} \sin(\varphi) \\ \sqrt{2} \cos(\varphi) - \sqrt{3} \sin(\varphi) \\ \sqrt{2} \cos(\varphi) \end{pmatrix}. \quad (\text{A2})$$

One-photon emission operator for $\mathbf{k}^{N\omega} \parallel [001]$:

$$O_D(\mathbf{E}^{N\omega}, \varphi) = \begin{pmatrix} -\sin(\varphi) \\ \cos(\varphi) \\ 0 \end{pmatrix}. \quad (\text{A3})$$

2. Two-photon excitation

Two-photon excitation operator for $\mathbf{k}_N^\omega \parallel [1\bar{1}0]$:

$$O_{DD}(\mathbf{E}_2^\omega, \psi) = \frac{1}{6\sqrt{2}} \times \begin{pmatrix} -4 \cos(2\psi) - \sqrt{2} \sin(2\psi) \\ -4 \cos(2\psi) - \sqrt{2} \sin(2\psi) \\ [\sqrt{2} \cos(\psi) + 2 \sin(\psi)]^2 \end{pmatrix}. \quad (\text{A4})$$

Two-photon excitation operator for $\mathbf{k}_N^\omega \parallel [11\bar{2}]$:

$$O_{DD}(\mathbf{E}_2^\omega, \psi) = \frac{1}{6\sqrt{2}} \times \begin{pmatrix} 2\sqrt{2} \cos(\psi)[\sqrt{2} \cos(\psi) - \sqrt{3} \sin(\psi)] \\ 2\sqrt{2} \cos(\psi)[\sqrt{2} \cos(\psi) + \sqrt{3} \sin(\psi)] \\ -1 + 5 \cos(2\psi) \end{pmatrix}. \quad (\text{A5})$$

Two-photon excitation operator for $\mathbf{k}_N^\omega \parallel [001]$:

$$O_{DD}(\mathbf{E}_2^\omega, \psi) = \begin{pmatrix} 0 \\ 0 \\ -\sqrt{2} \cos(\psi) \sin(\psi) \end{pmatrix}. \quad (\text{A6})$$

3. Three-photon excitation

Three-photon excitation operator for $\mathbf{k}_N^\omega \parallel [1\bar{1}0]$:

$$O_{DDD}(\mathbf{E}_3^\omega, \psi, A, C) = \frac{1}{12\sqrt{3}} \times \begin{pmatrix} [\sqrt{2}(5A - C)\cos^3(\psi) - 2(3A + C)\cos^2(\psi)\sin(\psi) + 4\sqrt{2}C\cos(\psi)\sin^2(\psi) - 8A\sin^3(\psi)] \\ [\sqrt{2}(5A - C)\cos^3(\psi) - 2(3A + C)\cos^2(\psi)\sin(\psi) + 4\sqrt{2}C\cos(\psi)\sin^2(\psi) - 8A\sin^3(\psi)] \\ 2[\sqrt{2}\cos(\psi) + \sin(\psi)][-3A - C + (A - C)[\cos(2\psi) + 2\sqrt{2}\sin(2\psi)]] \end{pmatrix}. \quad (\text{A7})$$

Three-photon excitation operator for $\mathbf{k}_N^\omega \parallel [11\bar{2}]$:

$$O_{DDD}(\mathbf{E}_3^\omega, \psi, A, C) = \frac{1}{24\sqrt{3}} \times \begin{pmatrix} [2\cos(\psi) + \sqrt{6}\sin(\psi)][4A\cos^2(\psi) + (3A + C)\sin^2(\psi) + \sqrt{6}(-A + C)\sin(2\psi)] \\ [2\cos(\psi) - \sqrt{6}\sin(\psi)][7A + C + (A - C)[\cos(2\psi) + 2\sqrt{6}\sin(2\psi)]] \\ -4\cos(\psi)[-5A + C + (A - C)\cos(2\psi)] \end{pmatrix}. \quad (\text{A8})$$

Three-photon excitation operator for $\mathbf{k}_N^\omega \parallel [001]$:

$$O_{\text{DDD}}(\mathbf{E}_3^\omega, \psi, A, C) = \frac{1}{6} \begin{pmatrix} [3A + C + 3(A - C)\cos(2\psi)]\sin(\psi) \\ \cos(\psi)[3A + C + 3(-A + C)\cos(2\psi)] \\ 0 \end{pmatrix}. \quad (\text{A9})$$

4. Four-photon excitation

Four-photon excitation operator for $\mathbf{k}_N^\omega \parallel [1\bar{1}0]$:

$$O_{\text{DDDD}}(\mathbf{E}_4^\omega, \psi) = \frac{1}{24\sqrt{6}} \begin{pmatrix} -2[-2\cos(\psi) + \sqrt{2}\sin(\psi)]^3[\cos(\psi) + \sqrt{2}\sin(\psi)] \\ -2[-2\cos(\psi) + \sqrt{2}\sin(\psi)]^3[\cos(\psi) + \sqrt{2}\sin(\psi)] \\ 9 + 7\cos(4\psi) + 4\sqrt{2}\sin(4\psi) \end{pmatrix}. \quad (\text{A10})$$

Four-photon excitation operator for $\mathbf{k}_N^\omega \parallel [11\bar{2}]$:

$$O_{\text{DDDD}}(\mathbf{E}_4^\omega, \psi) = -\frac{1}{36} \begin{pmatrix} [1 + 5\cos(2\psi)]\sin(\psi)[-3\cos(\psi) + \sqrt{6}\sin(\psi)] \\ [1 + 5\cos(2\psi)]\sin(\psi)[3\cos(\psi) + \sqrt{6}\sin(\psi)] \\ \sqrt{6}\sin^2(\psi)[1 + 5\cos(2\psi)] \end{pmatrix}. \quad (\text{A11})$$

Four-photon excitation operator for $\mathbf{k}_N^\omega \parallel [001]$:

$$O_{\text{DDDD}}(\mathbf{E}_4^\omega, \psi) = \begin{pmatrix} 0 \\ 0 \\ 0 \end{pmatrix}. \quad (\text{A12})$$

-
- [1] P. A. Franken, A. E. Hill, C. W. Peters, and G. Weinreich, Generation of Optical Harmonics, *Phys. Rev. Lett.* **7**, 118 (1961).
- [2] Y. R. Shen, *The Principles of Nonlinear Optics* (Wiley, New York, 1984).
- [3] R. W. Boyd, *Nonlinear Optics* (Elsevier, Amsterdam, 2008).
- [4] D. R. Yakovlev, V. V. Pavlov, A. V. Rodina, R. V. Pisarev, J. Mund, W. Warkentin, and M. Bayer, Exciton spectroscopy of semiconductors by the method of optical harmonics generation (review), *Phys. Solid State* **60**, 1471 (2018).
- [5] V. V. Pavlov, A. M. Kalashnikova, R. V. Pisarev, I. Sanger, D. R. Yakovlev, and M. Bayer, Magnetic-Field-Induced Second-Harmonic Generation in Semiconductor GaAs, *Phys. Rev. Lett.* **94**, 157404 (2005).
- [6] I. Sanger, D. R. Yakovlev, B. Kaminski, R. V. Pisarev, V. V. Pavlov, and M. Bayer, Orbital quantization of electronic states in a magnetic field as the origin of second-harmonic generation in diamagnetic semiconductors, *Phys. Rev. B* **74**, 165208 (2006).
- [7] M. Lafrentz, D. Brunne, A. V. Rodina, V. V. Pavlov, R. V. Pisarev, D. R. Yakovlev, A. Bakin, and M. Bayer, Second-harmonic generation spectroscopy of excitons in ZnO, *Phys. Rev. B* **88**, 235207 (2013).
- [8] J. Mund, D. Frohlich, D. R. Yakovlev, and M. Bayer, High-resolution second harmonic generation spectroscopy with femtosecond laser pulses on excitons in Cu₂O, *Phys. Rev. B* **98**, 085203 (2018).
- [9] A. Farenbruch, J. Mund, D. Frohlich, D. R. Yakovlev, M. Bayer, M. A. Semina, and M. M. Glazov, Magneto-Stark and Zeeman effect as origin of second harmonic generation of excitons in Cu₂O, *Phys. Rev. B* **101**, 115201 (2020).
- [10] D. Brunne, M. Lafrentz, V. V. Pavlov, R. V. Pisarev, A. V. Rodina, D. R. Yakovlev, and M. Bayer, Electric field effect on optical harmonic generation at the exciton resonances in GaAs, *Phys. Rev. B* **92**, 085202 (2015).
- [11] W. Warkentin, J. Mund, D. R. Yakovlev, V. V. Pavlov, R. V. Pisarev, A. V. Rodina, M. A. Semina, M. M. Glazov, E. L. Ivchenko, and M. Bayer, Third harmonic generation on exciton-polaritons in bulk semiconductors subject to a magnetic field, *Phys. Rev. B* **98**, 075204 (2018).
- [12] J. J. Hopfield and D. G. Thomas, Theoretical and experimental effects of spatial dispersion on the optical properties of crystals, *Phys. Rev.* **132**, 563 (1963).
- [13] C. F. Klingshirn, *Semiconductor Optics* (Springer, Berlin, 2012).
- [14] D. Frohlich, E. Mohler, and P. Wiesner, Observation of Exciton Polariton Dispersion in CuCl, *Phys. Rev. Lett.* **26**, 554 (1971).
- [15] D. C. Haueisen and H. Mahr, Observation of the dispersion curve of CuCl with second harmonic generation, *Phys. Lett. A* **36**, 433 (1971).
- [16] D. C. Haueisen and H. Mahr, Nonlinear Electronic Dispersion in CuCl, *Phys. Rev. Lett.* **26**, 838 (1971).
- [17] D. C. Haueisen and H. Mahr, Resonant second harmonic generation in the exciton region of CuCl and ZnO, *Phys. Rev. B* **8**, 734 (1973).
- [18] S. D. Kramer, F. G. Parsons, and N. Bloembergen, Interference of third-order light mixing and second-harmonic exciton generation in CuCl, *Phys. Rev. B* **9**, 1853 (1974).

- [19] B. F. Levine, R. C. Miller, and W. A. Nordland, Jr., Resonant exciton nonlinearities with spatial dispersion, *Phys. Rev. B* **12**, 4512 (1975).
- [20] D. Fröhlich, Two- and three-photon spectroscopy of solids, in *Nonlinear Spectroscopy of Solids: Advances and Applications*, edited by B. Di Bartolo and B. Bowlby (Plenum, New York, 1994), pp. 289–326.
- [21] S. Feierabend and H. G. Weber, Magnetoreflexion of S-excitons in cubic ZnSe, *Solid State Commun.* **26**, 191 (1978).
- [22] H. Mayer, U. Rössler, S. Permogorov, H. Stolz, H. Vogelsang, and W. von der Osten, Resonant Brillouin scattering in biaxially strained ZnSe, *J. Cryst. Growth* **138**, 195 (1994).
- [23] B. Sermage and G. Fishman, Resonant Brillouin Scattering of Polaritons in ZnSe: Heavy and Light Excitons, *Phys. Rev. Lett.* **43**, 1043 (1979).
- [24] B. Sermage and G. Fishman, Excitons and polaritons in ZnSe, *Phys. Rev. B* **23**, 5107 (1981).
- [25] Y. Nozue, M. Itho, and K. Cho, Excitonic polariton dispersion in ZnSe determined by the resonant Raman scattering under two-photon excitation of excitonic molecules, *J. Phys. Soc. Jpn.* **50**, 889 (1981).
- [26] F. Bogani, L. Carraresi, A. Filoramo, and S. Savasta, Exciton-polariton relaxation in ZnSe single crystals, *Phys. Rev. B* **46**, 9461 (1992).
- [27] D. Fröhlich, W. Nieswand, U. W. Pohl, and J. Wrzesinski, Two-photon spectroscopy of ZnSe under uniaxial strain, *Phys. Rev. B* **52**, 14652 (1995).
- [28] M. Sondergeld and R. G. Stafford, Exciton Fine Structure via Envelope-Hole Coupling in Cubic ZnSe, *Phys. Rev. Lett.* **35**, 1529 (1975).
- [29] F. Minami, K. Inoue, Y. Kato, K. Yoshida, and K. Era, Observation of the Forbidden Second Harmonic Generation in Resonance with 2P Wannier Exciton in ZnSe Thin Films, *Phys. Rev. Lett.* **67**, 3708 (1991).
- [30] M. Sondergeld, Two-photon absorption by envelope-hole coupled exciton states in cubic ZnSe. I. Energy spectrum of the H_d term and valence-band parameters, *Phys. Status Solidi B* **81**, 253 (1977).
- [31] M. Sondergeld, Two-photon absorption by envelope-hole coupled exciton states in cubic ZnSe. II. Polarization dependence in the case of degenerate valence bands, *Phys. Status Solidi B* **81**, 451 (1977).
- [32] H. W. Hölscher, A. Nöthe, and Ch. Uihlen, Investigation of band masses and g values of ZnSe by two-photon magnetoabsorption, *Phys. Rev. B* **31**, 2379 (1985).
- [33] K. Reimann and M. Steube, Nonlinear optical spectroscopy of semiconductors under pressure, *Phys. Status Solidi B* **211**, 189 (1999).
- [34] H. P. Wagner, M. Kühnelt, W. Langbein, and J. M. Hvam, Dispersion of the second-order nonlinear susceptibility in ZnTe, ZnSe, and ZnSe, *Phys. Rev. B* **58**, 10494 (1998).
- [35] J. Mund, Ch. Uihlein, D. Fröhlich, D. R. Yakovlev, and M. Bayer, Second harmonic generation on the yellow 1S exciton in Cu_2O in symmetry-forbidden geometries, *Phys. Rev. B* **99**, 195204 (2019).
- [36] S. I. Pekar, The theory of electromagnetic waves in a crystal in which excitons are produced, *J. Exptl. Theoret. Phys. (U.S.S.R.)* **33**, 1022 (1957).
- [37] D. D. Sell, S. E. Stokowski, R. Dingle, and J. V. DiLorenzo, Polariton Reflectance and Photoluminescence in High-Purity GaAs, *Phys. Rev. B* **7**, 4568 (1973).
- [38] M. Wörz, E. Giebl, Th. Reisinger, R. Flierl, B. Haserer, T. Semmler, T. Frey, and W. Gebhardt, Gap energies, exciton binding energies and band offsets in ternary ZnMgSe compounds and ZnSe/ZnMgSe heterostructures, *Phys. Status Solidi B* **202**, 805 (1997).
- [39] Ch. Uihlein, D. Fröhlich, and R. Kenklies, Investigation of exciton fine structure in Cu_2O , *Phys. Rev. B* **23**, 2731 (1981).
- [40] H. H. Li, Refractive index of ZnS, ZnSe, and ZnTe and its wavelength and temperature derivatives, *J. Phys. Chem. Ref. Data* **13**, 103 (1984).
- [41] *Properties of the Thirty-Two Point Groups*, edited by G. F. Koster, J. O. Dimmock, R. G. Wheeler, and H. Statz (MIT Press, Cambridge, MA, 1963).